






A series of tetranuclear [Ln₄] clusters with defect-dicubane cores including a Dy₄ single-molecule magnet

Haifeng Zhang, Jin Zhang, Yahong Li, Yaru Qin, Yanmei Chen, Wei Liu, Dandan Gao & Wu Li

To cite this article: Haifeng Zhang, Jin Zhang, Yahong Li, Yaru Qin, Yanmei Chen, Wei Liu, Dandan Gao & Wu Li (2015) A series of tetranuclear [Ln₄] clusters with defect-dicubane cores including a Dy₄ single-molecule magnet, Journal of Coordination Chemistry, 68:16, 2798-2809, DOI: [10.1080/00958972.2015.1067691](https://doi.org/10.1080/00958972.2015.1067691)


To link to this article: <http://dx.doi.org/10.1080/00958972.2015.1067691>

 View supplementary material 

 Accepted author version posted online: 03 Jul 2015.
Published online: 29 Jul 2015.

 Submit your article to this journal 

 Article views: 80

 View related articles 

 View Crossmark data 

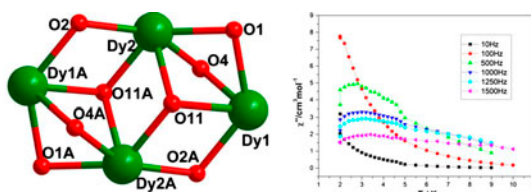
A series of tetranuclear [Ln₄] clusters with defect-dicubane cores including a Dy₄ single-molecule magnet

HAIFENG ZHANG[†], JIN ZHANG[†], YAHONG LI^{*†}, YARU QIN[†], YANMEI CHEN^{†‡},
WEI LIU[†], DANDAN GAO[‡] and WU LI[‡]

[†]College of Chemistry, Chemical Engineering and Materials Science, Soochow University, Suzhou, China

[‡]Qinghai Institute of Salt Lakes, Chinese Academy of Sciences, Xining, China

(Received 30 November 2014; accepted 8 June 2015)



A series of tetranuclear lanthanide compounds have been prepared. The Dy₄ complex exhibits single-molecule magnet behavior.

A series of tetranuclear lanthanide compounds, [Ln₄(μ₃-OH)₂L₄(NO₃)₂(DMF)₂] (H₂L = 2-(2-hydroxy-3-methoxybenzylideneamino)phenol; Ln = Dy (1); Tb (2); Er (3); and Gd (4)), have been prepared under hydrothermal conditions. X-ray crystal structure analysis reveals that 1–4 are polymorphs. The cores of the structures can be described as co-planar defect-dicubane. The solid-state luminescent properties indicate that the Ln^{III} ions have very deep influence on the luminescence of H₂L. The magnetic properties for 1–4 were studied. The Dy₄ complex exhibits single-molecule magnet behavior.

Keywords: Single-molecule magnet; Defect-dicubane; Luminescent property; Lanthanide ions

1. Introduction

Single-molecule magnet (SMM) is a magnet whose magnetic moments can be unified to a directional orientation under the influence of external magnetic field. When the external magnetic field is removed, the speed of the spin magnetic moment of molecular reorientation is very slow if the temperature is low enough [1–3]. Thus, the SMM has potential applications in high-density magnetic memory, molecular spintronics, and quantum computing devices [4]. Since the first SMM [5] was discovered in 1993, the design and synthesis of SMMs have received considerable attention. An SMM with higher energy barrier to

*Corresponding author. Email: liyahong@suda.edu.cn

magnetization reversal depends on a ground state with large negative axial magnetic anisotropy (D) and the total spin number of a ground state (S). Thus, there are many attempts to increase S and D [6, 7]. Recent advances in this area reveal that coordination compounds of lanthanide ions (especially Dy^{3+} , Tb^{3+} , and Er^{3+}) are candidates for SMMs due to their unquenched orbital angular momentum and large intrinsic magnetic anisotropy [8, 9]. A large number of lanthanide SMMs with various nuclearities have been reported [10–20]. Another important strategy for increasing S is to employ multidentate ligands which could incorporate many metal ions into one molecule. Multidentate hydroxyl-containing or carboxylate-containing Schiff base compounds are good ligands to construct SMMs [9].

In continuation of our recent work preparing lanthanide SMMs by employing Schiff base ligands [21, 22], we expand our efforts by exploring the reactions of lanthanide nitrates with 2-(2-hydroxy-3-methoxybenzylideneamino)phenol (H_2L). The employment of H_2L had previously given a series of $\text{Ni}^{\text{II}}/\text{Ln}^{\text{III}}$ [23–25], $\text{Co}^{\text{II}}/\text{Dy}^{\text{III}}$ [26], $\text{Fe}^{\text{III}}/\text{Ln}^{\text{III}}$ [27], and $\text{Mn}^{\text{III}}/\text{Ln}^{\text{III}}$ [28] heterometallic complexes, but few examples of homometallic clusters are also reported [29]. Thus, we conducted the reaction of lanthanide nitrates with H_2L . Four complexes, $[\text{Ln}_4(\mu_3\text{-OH})_2\text{L}_4(\text{NO}_3)_2(\text{DMF})_2]$ ($\text{Ln} = \text{Dy}$ (**1**); Tb (**2**); Er (**3**); and Gd (**4**)), were generated. The structures can be described as co-planar defect-dicubane. The solid-state luminescent properties of **1–4** indicate that the Ln^{III} ions have significant influence on the luminescent property of H_2L . The magnetic property investigations of **1–4** reveal that **1** displays typical features of SMMs. Herein, we report the synthesis, structures, luminescent, and magnetic properties of these four clusters.

2. Experimental

All solvents and reagents were of analytical grade and used as purchased. The Schiff-base ligand (H_2L) was synthesized using the reported procedure [30].

2.1. Synthesis of complexes

2.1.1. $[\text{Dy}_4(\mu_3\text{-OH})_2\text{L}_4(\text{NO}_3)_2(\text{DMF})_2]$ (1**).** A mixture of $\text{Dy}(\text{NO}_3)_3 \cdot 6\text{H}_2\text{O}$ (0.0456 g, 0.1 mmol), H_2L (0.0243 g, 0.1 mmol), NaOH (0.008 g, 0.2 mmol), MeOH (2 mL), and DMF (0.5 mL) was sealed in a Pyrex-tube (8 mL). The tube was heated for 12 h at 100 °C. After cooling to room temperature, red crystals of **1** were obtained in 40% yield (0.0192 g) based on Dy. Anal. Calcd for $\text{C}_{62}\text{H}_{60}\text{Dy}_4\text{N}_8\text{O}_{22}$ (%): C, 38.80; H, 3.15; N, 5.84. Found: C, 39.01; H, 3.24; N, 5.69. Selected IR data (KBr, cm^{-1}): 1645 (s), 1606 (m), 1583 (w), 1496 (m), 1479 (m), 1463 (s), 1381 (m), 1257 (m), 1226 (m), 970 (w), 819 (m), 742 (m), 736 (m), 680 (w), and 588 (w).

2.1.2. $[\text{Tb}_4(\mu_3\text{-OH})_2\text{L}_4(\text{NO}_3)_2(\text{DMF})_2]$ (2**).** Complex **2** was obtained by the same procedure as that of **1** using $\text{Tb}(\text{NO}_3)_3 \cdot 6\text{H}_2\text{O}$ in place of $\text{Dy}(\text{NO}_3)_3 \cdot 6\text{H}_2\text{O}$. Yield of **2** is 49% (0.0233 g) based on Tb. Anal. Calcd for $\text{C}_{62}\text{H}_{60}\text{Tb}_4\text{N}_8\text{O}_{22}$ (%): C, 39.09; H, 3.17; N, 5.88. Found: C, 38.85; H, 3.38; N, 5.91. Selected IR data (KBr, cm^{-1}): 1645 (s), 1606 (m), 1583 (w), 1496 (m), 1479 (m), 1462 (s), 1381 (m), 1257 (m), 1224 (m), 970 (w), 819 (m), 742 (m), 736 (m), 680 (w), and 588 (w).

2.1.3. [Er₄(μ₃-OH)₂L₄(NO₃)₂(DMF)₂] (3). A mixture of Er(NO₃)₃·6H₂O (0.0443 g, 0.1 mmol), H₂L (0.0243 g, 0.1 mmol), NaOH (0.008 g, 0.2 mmol), MeOH (2 mL), and DMF (1.0 mL) was sealed in a Pyrex-tube (8 mL). The tube was heated for 12 h at 100 °C. After cooling to room temperature, red crystals of **3** were obtained in 46% yield (0.0223 g) based on Er. Anal. Calcd for C₆₂H₆₀Er₄N₈O₂₂ (%): C, 38.42; H, 3.12; N, 5.78. Found: C, 38.84; H, 3.41; N, 5.69. Selected IR data (KBr, cm⁻¹): 1465 (s), 1608 (m), 1583 (m), 1498 (m), 1481 (m), 1465 (s), 1381 (m), 1257 (m), 1226 (m), 970 (m), 821 (m), 744 (m), 736 (m), 680 (w), and 588 (w).

2.1.4. [Gd₄(μ₃-OH)₂L₄(NO₃)₂(DMF)₂] (4). A mixture of Gd(NO₃)₃·6H₂O (0.0451 g, 0.1 mmol), H₂L (0.0243 g, 0.1 mmol), NaOH (0.008 g, 0.2 mmol), EtOH (2 mL), and DMF (0.3 mL) was sealed in a Pyrex-tube (8 mL). The tube was heated for 12 h at 100 °C. After cooling to room temperature, red crystals of **4** were obtained in 36% yield (0.0171 g) based on Gd. Anal. Calcd for C₆₂H₆₀Gd₄N₈O₂₂ (%): C, 39.23; H, 3.19; N, 5.90. Found: C, 39.46; H, 3.11; N, 5.78. Selected IR data (KBr, cm⁻¹): 1645 (s), 1606 (m), 1583 (w), 1496 (m), 1479 (m), 1460 (s), 1371 (m), 1255 (m), 1224 (m), 970 (w), 817 (m), 742 (m), 736 (m), and 586 (w).

2.2. X-ray diffraction crystallography

The data collections for **1–4** were carried out on a Bruker Smart ApexII diffractometer equipped with a graphite monochromator utilizing MoKα radiation ($\lambda = 0.71073 \text{ \AA}$ at

Table 1. Crystal data and structure refinement for **1–4**.

	1	2	3	4
Empirical formula	C ₆₂ H ₆₀ N ₈ O ₂₂ Dy ₄	C ₆₂ H ₆₀ N ₈ O ₂₂ Tb ₄	C ₆₂ H ₆₀ N ₈ O ₂₂ Er ₄	C ₆₂ H ₆₀ N ₈ O ₂₂ Gd ₄
Formula weight	1919.18	1904.86	1938.22	1898.18
Temperature (K)	296.15	296.15	296.15	296.15
Crystal system	Monoclinic	Monoclinic	Monoclinic	Monoclinic
Space group	<i>P</i> 2 ₁ / <i>n</i>	<i>P</i> 2 ₁ / <i>n</i>	<i>P</i> 2 ₁ / <i>n</i>	<i>P</i> 2 ₁ / <i>n</i>
<i>a</i> (Å)	16.0661(10)	16.1025(16)	13.0729(9)	16.1633(15)
<i>b</i> (Å)	11.3162(7)	11.3276(11)	14.071(1)	11.3605(11)
<i>c</i> (Å)	17.9645(12)	17.9904(18)	18.2247(13)	18.0486(17)
α (Å)	90	90	90	90
β (°)	94.429(1)	94.6150(10)	101.727(1)	94.7640(1)
γ (°)	90	90	90	90
Volume (Å ³)	3256.3(4)	3270.9(6)	3282.4(4)	3302.7(5)
<i>Z</i>	2	2	2	2
μ (mm ⁻¹)	4.620	4.355	5.144	4.047
<i>F</i> (0 0 0)	1852.2	1848	1868.0	1840
ρ_{Calcd} (g cm ⁻³)	1.9552	1.934	1.9589	1.909
θ range for data collection (°)	2.20–27.45	2.27–27.55	2.28–27.49	2.42–27.46
Measd./independent	19,085/7419	7429/5795	19,069/7396	19,225/7463
<i>R</i> _{int} reflections	0.0224	0.0222	0.0195	0.0238
Data/restraints/parameters	7419/0/436	7429/1/441	7396/0/436	7463/0/437
Goodness-of-fit on <i>F</i> ²	1.036	0.994	1.027	1.001
Final <i>R</i> indexes [<i>I</i> ≥ 2σ (<i>I</i>)]	<i>R</i> ₁ = 0.0237, <i>wR</i> ₂ = 0.0497	<i>R</i> ₁ = 0.0241, <i>wR</i> ₂ = 0.0602	<i>R</i> ₁ = 0.0233, <i>wR</i> ₂ = 0.0543	<i>R</i> ₁ = 0.0218, <i>wR</i> ₂ = 0.0442
Final <i>R</i> indexes [all data]	<i>R</i> ₁ = 0.0410, <i>wR</i> ₂ = 0.0570	<i>R</i> ₁ = 0.0380, <i>wR</i> ₂ = 0.0699	<i>R</i> ₁ = 0.0305, <i>wR</i> ₂ = 0.0593	<i>R</i> ₁ = 0.0400, <i>wR</i> ₂ = 0.0491
Largest diff. peak/hole (e Å ⁻³)	0.94/−0.78	1.034/−0.556	0.91/−0.86	0.506/−0.393

296 K); the $\omega - 2\theta$ scan technique was applied. The structures were solved by direct methods using SHELXS-97 and refined on F^2 using full-matrix least-squares with SHELXL-97 [31, 32]. The details of the crystal parameters, data collection, and refinements for the complexes are summarized in table 1; selected bond lengths and angles with their estimated standard deviations are listed in tables S1 and S2 (see online supplemental material at <http://dx.doi.org/10.1080/00958972.2015.1067691>), respectively.

3. Results and discussion

3.1. Synthesis of $[Ln_4(\mu_3\text{-OH})_2L_4(\text{NO}_3)_2(\text{DMF})_2]$ (**1**)

As described in the experimental section, the reaction of $\text{Ln}(\text{NO}_3)_3 \cdot 6\text{H}_2\text{O}$ with H_2L in the presence of NaOH in a solvent mixture of MeOH (or EtOH for **4**) and DMF generated a red solution, from which tetranuclear Ln_4 cluster was isolated. The role of sodium hydroxide is important in regulation of pH of the reaction mixture. When the ratio of the ligand and sodium hydroxide is 1 : 1, a clear solution was produced. As this ratio was changed to 1 : 3, there is precipitation in the tube. Red crystals can be found in the tube when the ratio is 1 : 2. Moreover, the amount of DMF is also crucial in the formation of crystals. Excessive DMF leads to clear solution and precipitation resulted if the DMF is not enough.

Red crystals can also be synthesized when we carry out the reaction of $\text{Ln}(\text{NO}_3)_3 \cdot 6\text{H}_2\text{O}$ (0.1 mmol) with *o*-vanillin (0.1 mmol) and *o*-aminophenol (0.1 mmol) in the presence of NaOH (0.2 mmol) in a solvent mixture of MeOH (2 mL) (or EtOH for **4**) and DMF (0.5, or 1 mL for **3**, 0.3 mL for **4**) at 100 °C. The ligand 2-(2-hydroxy-3-methoxybenzylideneamino)phenol (H_2L) can be formed *in situ* from the reaction of *o*-vanillin and *o*-aminophenol.

3.2. Descriptions of the structures of **1–4**

Single-crystal X-ray diffraction reveals that **1–4** are polymorphs. Therefore, **1** is chosen to depict the structure in detail. Compound **1** crystallizes in the monoclinic space group $P2_1/n$. The asymmetric unit consists of two Dy^{III} ions, two L^{2-} , one OH^- , one nitrate, and one DMF [figure 1(a)]. The compound has an inversion center. Dy1 is eight-coordinate by one nitrogen and two phenolate oxygens from one L^{2-} , one methoxy oxygen, and one phenolate oxygen from another L^{2-} , one oxygen from OH^- ion, one oxygen from DMF, and one phenolate oxygen from the third L^{2-} ligand. The O7N donor sites around Dy1 adopt a distorted square-antiprismatic geometry. The coordination environments of Dy1 and Dy2 are slightly different. Dy2 also has an O7N sphere and displays a distorted square-antiprismatic geometry, with two oxygens from nitrate, two oxygens from two OH^- ions, one nitrogen, and two phenolate oxygens from one L^{2-} ligand, and one oxygen from another L^{2-} ligand [figure 1(b)].

The core of the complex can be described as a defect-dicubane (figure 2) and the coordination modes of the ligands are shown in scheme 1. The four coplanar Dy^{III} ions are bridged by two $\mu_3\text{-OH}$ ligands located on opposite sides of the Dy_4 plane with one $\mu_3\text{-OH}$ being above the Dy_4 plane (0.9502 Å), and the other one being below the Dy_4 plane. Each OH^- serves as a fairly symmetrical triple bridge, connecting Dy1 and Dy2, Dy2 and Dy2A, Dy1 and Dy2A, respectively, with Dy–O bond lengths of 2.399(2), 2.349(2), and 2.334(2) Å

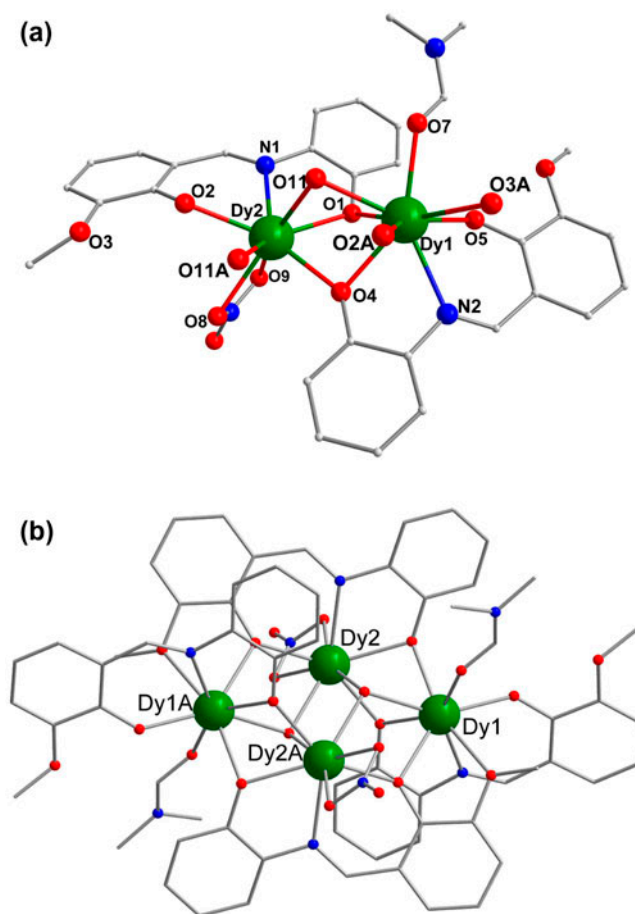


Figure 1. (a) Asymmetrical unit of **1** with partial labeling scheme and (b) molecular structure of **1** (hydrogens have been omitted for clarity).

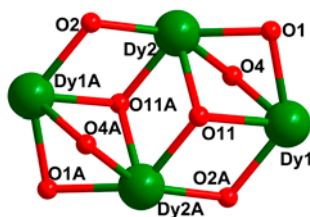


Figure 2. The Dy₄ unit of **1**.

and Dy–O–Dy angles of 110.30(10)°, 109.52(9)°, and 93.79(8)°. The phenolate oxygens also serve as bridging atoms, pairwise bridging the Dy ions to complete the defect-dicubane core.

Complex **1** joins a big family of Dy₄ clusters [33–44]. Several topologies for Dy₄ complexes have been found [29, 44]. However, the configurations of Dy₄ defect-dicubane are not common [12, 29, 40, 44].

3.3. Luminescent properties

The solid-state luminescent properties of **1–4** and H₂L at room temperature were investigated. The emission spectra of **1–4** and H₂L are shown in figure 3. The emission spectrum of H₂L was obtained by exciting the complex at 390 nm. It can be seen from figure 4 the emission spectrum consists of a broad band ranging from 530 to 740 nm with the maximum wavelength at 603 nm. For **4**, the maximum wavelength appeared at 560 nm when it was excited at 390 nm. The fluorescent properties of **1**, **2**, and **3** were much weaker than those of H₂L and **4**. The maximum wavelengths of **1–3** appear at 524, 536, and 504 nm, respectively. The emission peak of **4** shifts to lower wavelengths relative to the ligand, and the fluorescent properties of **1**, **2**, and **3** were nearly quenched. These phenomena can be attributed to the influence of metal ions on the ligand π – π^* transition [45]. The luminescence of **2** at 173 K was also investigated, and no emission was observed (figure S14).

3.4. Magnetic studies

Magnetism studies on coordination complexes of lanthanides are of continuing interest [46–50], since they can provide understanding of fundamental factors governing their magnetic properties. Some lanthanide complexes showed both luminescence and single-ion magnet (single-molecule magnetic) properties [51–53]. Thus, the magnetic properties of **1–4** were also investigated.

The temperature dependence of the molar magnetic susceptibility for **1–4** was performed on polycrystalline samples between 2 and 300 K in an applied magnetic field of 1000 Oe.

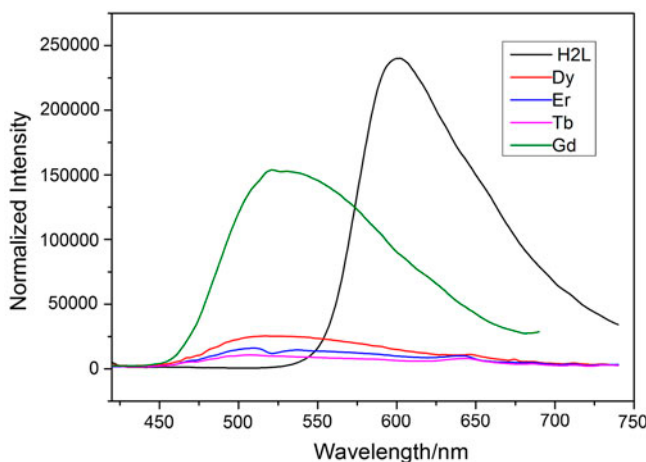


Figure 3. Emission spectra of **1–4** and H₂L (excited at 390 nm) in the solid state at room temperature.

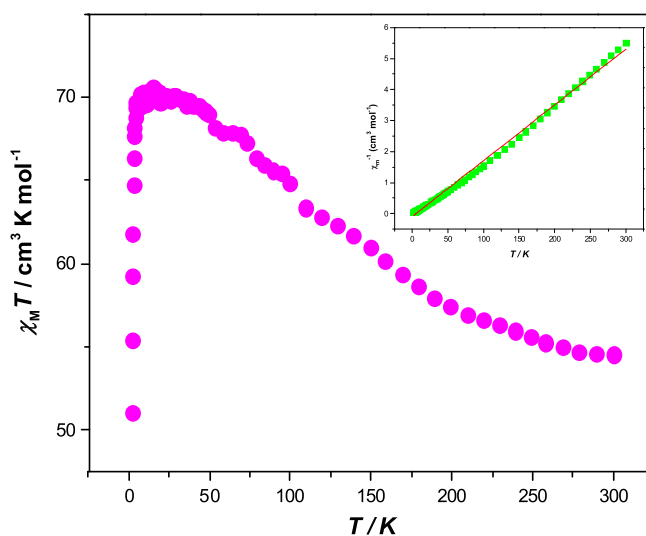


Figure 4. Temperature dependence of the $\chi_M T$ product from 2 to 300 K at 1000 Oe for **1**. The inset is the Curie–Weiss law fit from 300 to 2 K.

The room temperature, the $\chi_M T$ value of **1** is $54.55 \text{ cm}^3 \text{ K mol}^{-1}$ (figure 4), which is slightly lower than the value of $56.68 \text{ cm}^3 \text{ K mol}^{-1}$ expected for four uncoupled Dy^{III} ions (${}^6\text{H}_{15/2}$, $S = 5/2$, $L = 5$, and $g = 4/3$). Upon cooling, the $\chi_M T$ value rises gradually and reaches a maximum value of $70.59 \text{ cm}^3 \text{ K mol}^{-1}$ at 15 K and then decreases sharply to reach minimum of $51.01 \text{ cm}^3 \text{ K mol}^{-1}$ at 2 K, suggesting the presence of weak ferromagnetic interactions within the cluster. The ferromagnetic interactions were also confirmed by

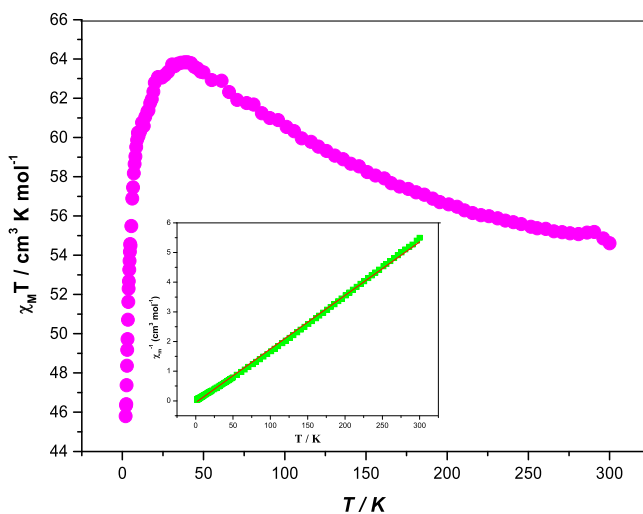


Figure 5. Temperature dependence of the $\chi_M T$ product from 2 to 300 K at 1000 Oe for **2**. The inset is the Curie–Weiss law fit from 300 to 2 K.

the Curie–Weiss analysis of the magnetic susceptibility data with $C = 54.27 \text{ cm}^3 \text{ K mol}^{-1}$ and $\theta = 5.1 \text{ K}$.

The observed $\chi_M T$ value of **2** is $54.61 \text{ cm}^3 \text{ K mol}^{-1}$ (figure 5), which is higher than the expected value of $47.28 \text{ cm}^3 \text{ K mol}^{-1}$ for uncoupled Tb^{III} ions (7F_6 , $S = 3$, $L = 3$, $g = 3/2$). As the temperature is lowered, the $\chi_M T$ value undergoes a gradual increase and reaches a maximum value of $63.83 \text{ cm}^3 \text{ mol}^{-1} \text{ K}$ at 40 K and then decreases sharply to reach minimum of $45.80 \text{ cm}^3 \text{ mol}^{-1} \text{ K}$ at 2 K. The phenomenon indicates the presence of dominant ferromagnetic exchange interactions between the metal ions. The ferromagnetic interactions were also confirmed by the Curie–Weiss analysis of the magnetic susceptibility data with $C = 55.41 \text{ cm}^3 \text{ K mol}^{-1}$ and $\theta = 3.0 \text{ K}$.

The temperature dependence of the magnetic susceptibilities for **3** and **4** are shown in figures 6 and 7. The corresponding values at room temperature are 43.24 and $32.07 \text{ cm}^3 \text{ K mol}^{-1}$ for **3** and **4**, respectively, slightly different with the expected paramagnetic values of 46.00 and $31.50 \text{ cm}^3 \text{ K mol}^{-1}$ for Er^{III} and Gd^{III} . The $\chi_M T$ products of **3** and **4** decrease gradually with the decreasing in temperature. In the case of **3**, the sharp decrease starts at 30 K before reaching the minimum value of $28.11 \text{ cm}^3 \text{ mol}^{-1} \text{ K}$ at 2 K. The sharp decrease of **4** begins at 25 K and reaches minimum of $12.16 \text{ cm}^3 \text{ mol}^{-1} \text{ K}$ at 2 K, revealing the antiferromagnetic interactions within the cluster. The antiferromagnetic interactions were confirmed by the Curie–Weiss analysis of the magnetic susceptibility data with $\theta = -2.8 \text{ K}$ for **3** and $\theta = -3.2 \text{ K}$ for **4**, respectively.

To further understand the magnetism of **1**, ac dynamic susceptibility measurements were performed under zero dc field at frequencies of 10, 100, 500, 1000, 1250, and 1500 Hz (figure 8). Strong out-of-phase signals were observed for **1**, which indicate slow relaxation of magnetization. These signals are indicative of SMM behavior.

A similar Dy_4 cluster, $[\text{Ln}^{\text{III}}_4(\mu_3\text{-OH})_2(\text{L})_4(\text{HL})_2] \cdot 2\text{THF}$, has been constructed by using the same ligand [29]. To our surprise, the dc and ac magnetic properties of **1** are totally

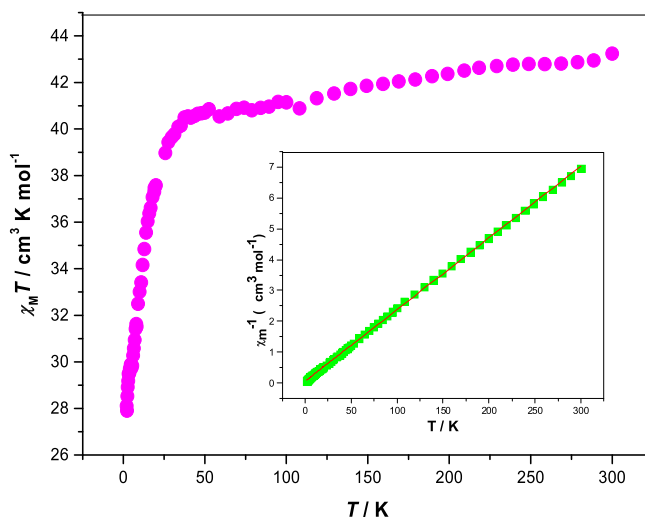


Figure 6. Temperature dependence of the $\chi_M T$ product from 2 to 300 K at 1000 Oe for **3**. The inset is the Curie–Weiss law fit from 300 to 2 K.

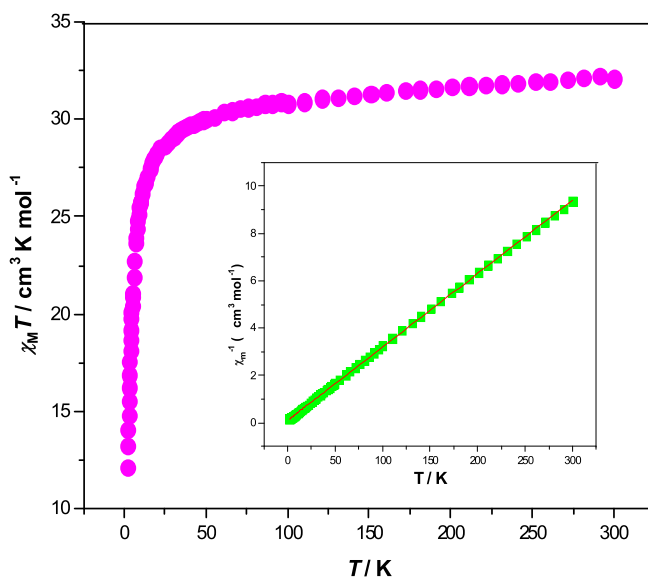


Figure 7. Temperature dependence of the $\chi_M T$ product from 2 to 300 K at 1000 Oe for **4**. The inset is the Curie–Weiss law fit from 300 to 2 K.

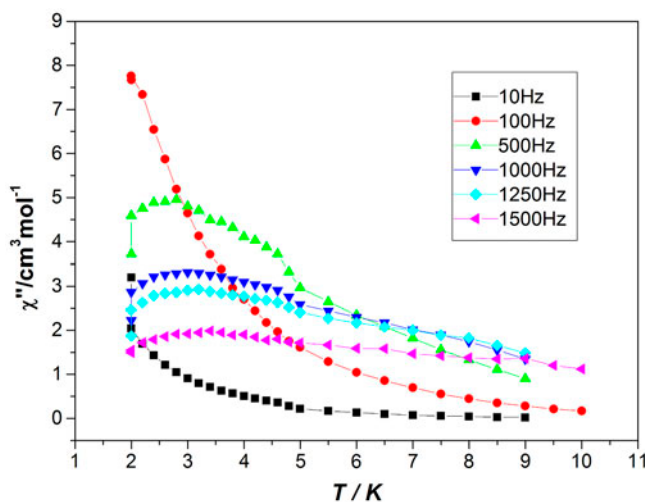
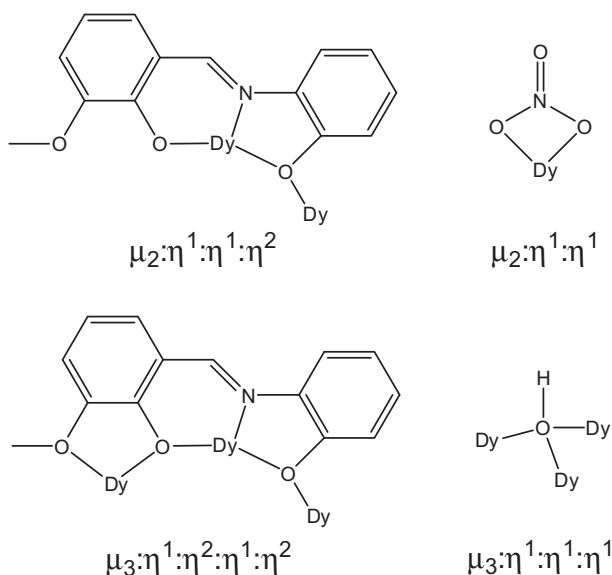


Figure 8. Frequency dependence of the out-of-phase (χ'') ac susceptibility under an applied zero Oe field for **1**.

different from those of $[\text{Ln}^{\text{III}}_4(\mu_3\text{-OH})_2(\text{L})_4(\text{HL})_2]\cdot 2\text{THF}$, indicating that the structural change could result in variation of the magnetic properties.

For **2**, the temperature-dependent (figures S8 and S9) ac susceptibility was also carried out under zero dc field. To our disappointment, no out-of-phase signal was observed, indicating that **2** does not exhibit the property of SMM.



Scheme 1. Coordination modes of the ligands in **1**.

4. Conclusion

Four tetranuclear lanthanide clusters have been prepared. The structures can be described as co-planar defect-dicubane. The luminescent and magnetic properties of **1–4** are also investigated. Complex **1** displays typical features of SMM.

Supplementary material

Tables S1 and S2 give bond lengths and angles for **1–4**. Figure S1 gives packing diagram for **1**. Figure S2 gives coordination polyhedrons around Dy1 and Dy2 ions of **1**. Figure S3 gives the XRD spectra for **1–4**. Figures S4–S7 give the IR spectra for **1–4**. Figures S8 and S9 give the magnetic properties for **2**. CCDC reference numbers are 1006750, 1032544, 1006751, and 1032545 for **1–4**, respectively. These data can be obtained free of charge from the Cambridge Crystallographic Data Center via http://www.ccdc.cam.ac.uk/data_request/cif, by e-mailing data_request@ccdc.cam.ac.uk or by contacting the Cambridge Crystallographic Data Center, 12 Union Road, Cambridge CB2 1EZ, UK; Fax: +44(0)1223 336033.

Disclosure statement

No potential conflict of interest was reported by the authors.

Funding

This work was supported by the National Natural Science Foundation of China [grant number 21272167], [grant number 21201127]; Priority Academic Program Development of Jiangsu Higher Education Institution; KLSLRC [grant number KLSLRC-KF-13-HX-1].

References

- [1] C.P. Landee, M.M. Turnbull. *J. Coord. Chem.*, **67**, 375 (2014).
- [2] Y.N. Guo, G.F. Xu, Y. Guo, J.K. Tang. *Dalton Trans.*, **40**, 9953 (2011).
- [3] L. Sorace, C. Benelli, D. Gatteschi. *Chem. Soc. Rev.*, **40**, 3092 (2011).
- [4] M. Cavallini, J. Gomez-Segura, D. Ruiz-Molina, M. Massi, C. Albonetti, C. Rovira, J. Veciana, F. Biscarini. *Angew. Chem. Int. Ed.*, **44**, 888 (2005).
- [5] R. Sessoli, D. Gatteschi, A. Caneschi, M.A. Novak. *Nature*, **365**, 141 (1993).
- [6] M. Soler, W. Wernsdorfer, K. Folting, M. Pink, G. Christou. *J. Am. Chem. Soc.*, **126**, 2156 (2004).
- [7] B.H. Koo, K.S. Lim, D.W. Ryu, W.R. Lee, E.K. Kohb, C.S. Hong. *Chem. Commun.*, **48**, 2519 (2012).
- [8] D.N. Woodruff, R.E.P. Winpenney, R.A. Layfield. *Chem. Rev.*, **113**, 5110 (2013).
- [9] P. Zhang, Y.N. Guo, J.K. Tang. *Coord. Chem. Rev.*, **257**, 1728 (2013).
- [10] Y.N. Guo, G.F. Xu, W. Wernsdorfer, L. Ungur, Y. Guo, J.K. Tang, H.J. Zhang, L.F. Chibotaru, A.K. Powell. *J. Am. Chem. Soc.*, **133**, 11948 (2011).
- [11] L.J. Hewitt, Y.H. Lan, C.E. Anson, J. Luzon, R. Sessoli, A.K. Powell. *Chem. Commun.*, **44**, 6765 (2009).
- [12] Y.Z. Zheng, Y.H. Lan, C.E. Anson, A.K. Powell. *Inorg. Chem.*, **47**, 10813 (2008).
- [13] M.T. Gamer, Y. Lan, P.W. Roesky, A.K. Powell, R. Clérac. *Inorg. Chem.*, **47**, 6581 (2008).
- [14] H.Q. Tian, M. Wang, L. Zhao, Y.N. Guo, Y. Guo, J.K. Tang, Z.L. Liu. *Chem. Eur. J.*, **18**, 442 (2012).
- [15] A.B. Canaj, D.I. Tzimopoulos, A. Philippidis, E.G. Kostakis, C.J. Milios. *Inorg. Chem.*, **51**, 7451 (2012).
- [16] H.Q. Tian, L. Zhao, Y.N. Guo, Y. Guo, J.K. Tang, Z.L. Liu. *Chem. Commun.*, **48**, 708 (2012).
- [17] D.I. Alexandropoulos, S. Mukherjee, C. Papatriantafyllopoulou, C.P. Raptopoulou, V. Psycharis, V. Bekiari, G. Christou, T.C. Stamatatos. *Inorg. Chem.*, **50**, 11276 (2011).
- [18] H.S. Ke, G.F. Xu, L. Zhao, J.K. Tang, X.Y. Zhang, H.J. Zhang. *Chem. Eur. J.*, **15**, 10335 (2009).
- [19] Y.L. Miao, J.L. Liu, J.Y. Li, J.D. Leng, Y.C. Ou, M.L. Tong. *Dalton Trans.*, **40**, 10229 (2011).
- [20] L. Zhao, S.F. Xue, J.K. Tang. *Inorg. Chem.*, **51**, 5994 (2012).
- [21] S.X. She, M.J. Zaworotko, W. Liu, Z.X. Zhang, Y.H. Li. *Crystallogr. Eng. Commun.*, **15**, 5003 (2013).
- [22] S.X. She, Y.M. Chen, M.J. Zaworotko, W. Liu, Y.Y. Cao, J. Wu, Y.H. Li. *Dalton Trans.*, **42**, 10433 (2013).
- [23] K.C. Mondal, G.E. Kostakis, Y. Lan, W. Wernsdorfer, C.E. Anson, A.K. Powell. *Inorg. Chem.*, **50**, 11604 (2011).
- [24] H. Ke, L. Zhao, Y. Guo, J. Tang. *Inorg. Chem.*, **51**, 2699 (2012).
- [25] H. Ke, S. Zhang, W. Zhu, G. Xie, S. Chen. *J. Coord. Chem.*, **68**, 808 (2015).
- [26] K.C. Mondal, A. Sundt, Y. Lan, G.E. Kostakis, O. Waldmann, L. Ungur, L.F. Chibotaru, C.E. Anson, A.K. Powell. *Angew. Chem. Int. Ed.*, **51**, 7550 (2012).
- [27] I. Nemeč, M. Machata, R. Herchel, R. Boča, Z. Trávníček. *Dalton Trans.*, **41**, 14603 (2012).
- [28] H. Ke, W. Zhu, S. Zhang, G. Xie, S. Chen. *Polyhedron*, **87**, 109 (2015).
- [29] K.C. Mondal, G.E. Kostakis, Y. Lan, A.K. Powell. *Polyhedron*, **66**, 268 (2013).
- [30] Y.H. Fan, C.F. Bi, J.Y. Li. *J. Radioanal. Nucl. Chem.*, **254**, 641 (2002).
- [31] G.M. Sheldrick. *SHELXS-97, Program for Crystal Structure Solution*, University of Göttingen, Germany (1997).
- [32] G.M. Sheldrick. *SHELXL-97, Program for the Refinement of Crystal Structures from Diffraction Data*, University of Göttingen, Germany (1997).
- [33] P.H. Guo, Y. Meng, Y.C. Chen, Q.W. Li, B.Y. Wang, J.D. Leng, D.H. Bao, J.H. Jia, M.L. Tong. *J. Mater. Chem. C*, **2**, 8858 (2014).
- [34] S.F. Xue, Y.N. Guo, L. Zhao, P. Zhang, J.K. Tang. *Dalton Trans.*, **43**, 1564 (2014).
- [35] V. Chandrasekhar, S. Das, A. Dey, S. Hossain, J.P. Sutter. *Inorg. Chem.*, **52**, 11956 (2013).
- [36] C.M. Liu, D.Q. Zhang, D.B. Zhu. *Dalton Trans.*, **42**, 14813 (2013).
- [37] S.Q. Wu, Q.W. Xie, G.Y. An, X. Chen, C.M. Liu, A.L. Cui, H.Z. Kou. *Dalton Trans.*, **42**, 4369 (2013).
- [38] S.F. Xue, L. Zhao, Y.N. Guo, X.H. Chen, J.K. Tang. *Chem. Commun.*, **48**, 7031 (2012).
- [39] P.H. Guo, J.L. Liu, Z.M. Zhang, L. Ungur, L.F. Chibotaru, J.D. Leng, F.S. Guo, M.L. Tong. *Inorg. Chem.*, **51**, 1233 (2012).
- [40] P.F. Yan, P.H. Lin, F. Habib, T. Aharen, M. Murugesu, Z.P. Deng, G.M. Li, W.B. Sun. *Inorg. Chem.*, **50**, 7059 (2011).
- [41] P.H. Lin, L. Korobkov, W. Wernsdorfer, L. Ungur, L.F. Chibotaru, M. Murugesu. *Eur. J. Inorg. Chem.*, **10**, 1535 (2011).
- [42] P.P. Yang, X.F. Gao, H.B. Song, S. Zhang, X.L. Mei, L.C. Li, D.Z. Liao. *Inorg. Chem.*, **50**, 720 (2011).

- [43] G. Abbas, Y.H. Lan, G.E. Kostakis, W. Wernsdorfer, C.E. Anson, A.K. Powell. *Inorg. Chem.*, **49**, 8067 (2010).
- [44] S.Y. Lin, J.K. Tang. *Polyhedron*, **83**, 185 (2014).
- [45] F.L. Hu, X.H. Yin, J. Lu, Y. Mi, J.C. Zhuang, W.Q. Luo. *J. Coord. Chem.*, **63**, 263 (2010).
- [46] C. Wang, Y.L. Wang, Y. Ma, Q.L. Wang, L.C. Li, D.Z. Liao. *J. Coord. Chem.*, **65**, 2830 (2012).
- [47] X.L. Wang. *J. Coord. Chem.*, **64**, 4334 (2011).
- [48] M.H. Yu, X.B. Wang, M. Hu. *J. Coord. Chem.*, **68**, 520 (2015).
- [49] N. Wang, S.T. Yue, Y.L. Liu. *J. Coord. Chem.*, **62**, 1914 (2009).
- [50] F.M. Ramírez, M.E. Sosa-torres, R. Escudero, J. Padilla, J.A. Ascencio. *J. Coord. Chem.*, **50**, 1 (2000).
- [51] J. Long, R. Vallat, R.A.S. Ferreira, L.D. Carlos, F.A. Almeida, Y. Guari, J. Larionova. *Chem. Commun.*, **48**, 9974 (2012).
- [52] G. Cucinotta, M. Perfetti, J. Luzon, M. Etienne, P. Car, A. Caneschi, G. Calvez, K. Bernot, R. Sessoli. *Angew. Chem. Int. Ed.*, **51**, 1606 (2012).
- [53] J. Ruiz, A.J. Mota, A. Rodríguez-Diéguez, S. Titos, J.M. Herrera, E. Ruiz, E. Cremades, J.P. Costes, E. Colacio. *Chem. Commun.*, **48**, 7916 (2012).